ELSEVIER

Chemical Engineering Journal 127 (2007) 1–9

Chemical Engineering Journal

www.elsevier.com/locate/cej

# Influence of the temperature on the properties of the soot formed from $C_2H_2$ pyrolysis

M.P. Ruiz [a,*], R. Guzmán de Villoria [b], A. Millera [a], M.U. Alzueta [a], R. Bilbao [a]

[a] *Aragón Institute of Engineering Research, Department of Chemical and Environmental Engineering, University of Zaragoza, Campus Río Ebro, C/María de Luna 3, 50018 Zaragoza, Spain*

[b] *Department of Mechanical Engineering, University of Zaragoza, Campus Río Ebro, C/María de Luna 3, 50018 Zaragoza, Spain*

Received 13 July 2006; received in revised form 11 September 2006; accepted 12 September 2006

**Abstract**

The influence of temperature on the properties of the soot formed from $C_2H_2$ pyrolysis has been studied. Pyrolysis experiments were carried out in a quartz reactor at 1000–1200 °C, for an inlet $C_2H_2$ concentration of 15,000 ppmv. Outlet gases were analysed by gas chromatography and the amount of soot produced measured. The soot samples formed were further characterized using elemental analysis, BET surface area, transmission electron microscopy, X-ray photoelectron spectroscopy, X-ray diffraction and Raman spectroscopy. The soot reactivity towards $O_2$ and NO was studied. Results show that formation temperature is a key parameter in the properties and reactivities of the soot samples formed. The higher the temperature the less reactive the soot, and structural properties support these results.


*Keywords:* Soot; Transmission electron microscopy; X-ray diffraction; Raman spectroscopy; Reactivity

## 1. Introduction

Soot is a carbonaceous solid produced during the combustion of fuels when combustion conditions are sufficiently fuel-rich to allow polymerization/condensation reactions of the fuel to take place, so that the soot particle can nucleate and grow. Soot is an undesirable combustion product, and its formation represents one of the most complex chemical systems in combustion. Considerable progress has been made in recent years in understanding the chemical and physical aspects of soot formation in combustion processes. The process of soot evolution from fuel consists of complex chemical and physical steps, including fuel pyrolysis, polycyclic aromatic hydrocarbon (PAH) formation, particle inception, coagulation, surface growth, carbonization, agglomeration, and oxidation [1,2]. Soot emissions in combustion may be controlled by limiting the inception of new soot particles or by burn-out of existing soot particles. In this context, a study of the soot formation process and the properties and reactivity of the resultant soot samples in different conditions may be interesting to the development of strategies to control emissions.

The knowledge of the soot reactivity in different environments is of great significance for pollution control in combustion processes: industrial flames, auto engines, etc. In fact, the study of the interaction between soot and different gases is important, not only to eliminate the soot particles, but also to analyse the reduction of the NO generated in the combustion process [3–5].

The soot reactivity is directly related to its structure and composition. Properties such as surface area, particle size and crystallinity affect the reactivity of the soot particles. The soot nanostructure depends upon its formation conditions, like fuel identity, residence time and temperature. An understanding of these dependences is fundamental to control the physical properties of the soot and therefore, its chemical reactivity [6–9].

In order to analyse the physical properties of the soot and relate them further to its reactivity, different techniques have been widely used, mainly scattering and microscopic techniques. X-ray diffraction, Raman spectroscopy and transmission electron microscopy are current techniques used to study the soot nanostructure and morphology [10–17].

Motivated by all these issues, the purpose of this article is the study of the influence of the temperature on the formation, properties and reactivity of the soot formed from $C_2H_2$ pyrolysis, compound that is considered as the main precursor of soot.

* Corresponding author. Tel.: +34 976761150; fax: +34 976761879.
*E-mail address:* pilruiz@unizar.es (M.P. Ruiz).

1385-8947/$ – see front matter © 2006 Elsevier B.V. All rights reserved.
doi:10.1016/j.cej.2006.09.006

To do that, different techniques (elemental analysis, determination of BET area, transmission electron microscopy, X-ray photoelectron spectroscopy, X-ray diffraction and Raman spectroscopy) have been used to relate the formation temperature to the soot nanostructure and its reactivity towards $O_2$ and NO.

## 2. Experimental

### 2.1. Soot formation

Experiments of $C_2H_2$ pyrolysis have been carried out in the facility shown in Fig. 1. This installation is similar to the one employed in a previous work [18]. It consists of a gas feeding system, a reaction system, a soot collection system, and a gas analysis system. The reactor employed is a quartz tube of 45 mm internal diameter and 800 mm in length. Reactor inlet and outlet can be cooled, by an air flow, which allows controlling the temperature profile inside the reactor. Longitudinal temperature profiles inside the reactor have been determined by means of a S-type thermocouple in different conditions. The reactor is placed in an oven electrically heated. The soot formed in the reaction is collected in quartz fiber filters of 25 mm diameter and 60 mm in length, with a pore size less than 1 μm.

In the experiments, a given flow rate of $C_2H_2$ diluted in nitrogen is fed into the reaction system, which is heated at different temperatures in the 1000–1200 °C range. No soot formation has been observed at lower temperatures. The inlet $C_2H_2$ concentration used is 15,000 ppmv and the total flow rate is 1000 ml/min (STP). Taking into account the total flow rate used and the temperature interval considered, a length of the reaction zone of 14 cm can be assumed with a flat temperature profile ±25 °C. Thus, the gas residence time in these experiments, defined as the reaction zone volume divided by the total gas flow rate introduced, is $3983/T$ (K) s. Every experiment is run during the necessary time to collect a significant amount of soot (higher than 1 g). This results in a length of the experiment of about 3 h. In every experiment, the composition of the outlet gas has been analysed by gas chromatography and the soot obtained has been collected. For further soot reactivity study and analyses, and in order to eliminate the adsorbed compounds in the soot samples formed, the raw samples are annealed during 1 h in a $N_2$ atmosphere at 1100 °C, except the soot samples produced at 1000 and 1050 °C, which are annealed at their formation temperature to avoid possible structural changes.

### 2.2. Soot reactivity

In order to study the reactivity of the soot samples formed, experiments of the soot–$O_2$ and soot–NO interactions have been carried out in a quartz reactor for a temperature of 1000 °C and a total flow rate of 1000 ml/min (STP). For the soot–$O_2$ experiments, the inlet $O_2$ concentration used is 500 ppmv, and for the soot–NO tests, the inlet NO concentration is 2000 ppmv.

The experimental set-up used for the soot reactivity experiments is shown in Fig. 2. A control panel connected to mass flow controllers is used to prepare a mixture of gases ($N_2/O_2$ or $N_2$/NO) from gas cylinders. The desired mixture is directed to a quartz reactor of 550 mm in length and 15 mm internal diameter. It is heated by an electrical furnace.

For every experiment, the amount of soot introduced into the reactor is approximately 10 mg and it is always previously mixed with 350 mg of silica sand (150 μm). The mixture is located on a quartz wool plug placed in a bottleneck in the middle of the reactor, resulting in a thin layer. The sand is necessary to facilitate the introduction of the sample into the reactor and to prevent agglomeration of the soot particles. An inert flow of $N_2$ is fed while the sample is heated up to the reaction temperature (1000 °C). Once this set point is reached, the reactant gas mixture is fed. The reaction temperature is measured by a thermocouple placed 0.5 cm just below the quartz wool plug where the reac-

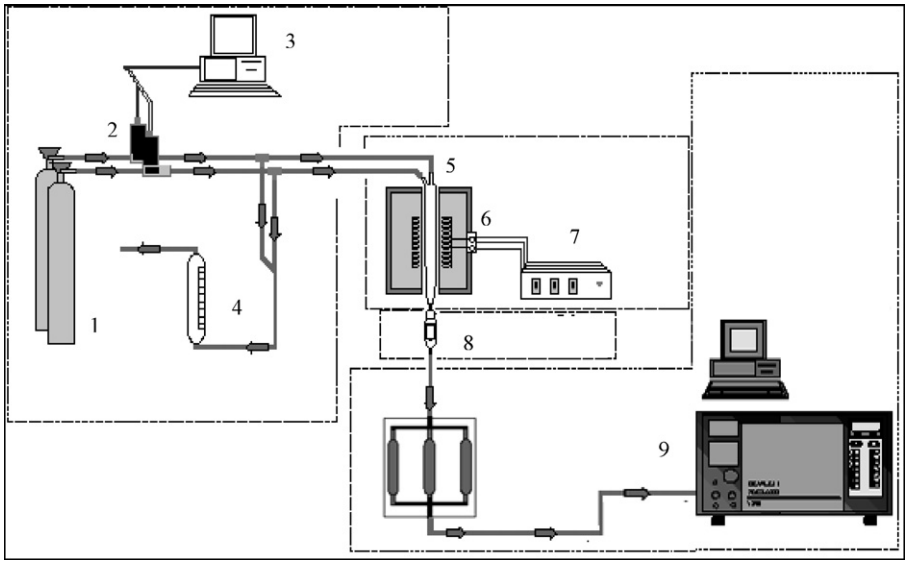


Fig. 1. Experimental set-up used for the $C_2H_2$ pyrolysis experiments. (1) $N_2$ and $C_2H_2$ cylinders; (2) mass flow meters; (3) control unit; (4) bubble flow meter; (5) quartz reactor; (6) electric furnace; (7) temperature controller; (8) soot sampling filter; (9) gas chromatograph.

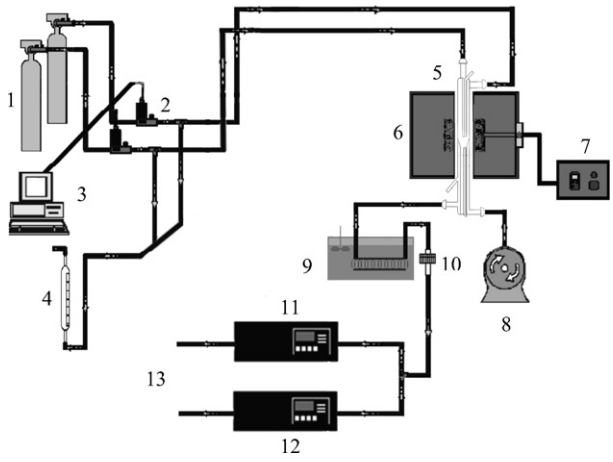


Fig. 2. Experimental set-up used for the soot–$O_2$ and soot–NO interaction tests. (1) $N_2$ and $O_2$ (or NO) cylinders; (2) mass flow meters; (3) control unit; (4) bubble flow meter; (5) fixed bed reactor; (6) electric furnace; (7) temperature controller; (8) compressor; (9) condenser; (10) particle filter; (11) NO analyser; (12) CO/$CO_2$ analyser; (13) vent.

tion takes place. The reaction products are evacuated and then cooled down to room temperature. Prior to the analysis system, a particle filter is placed in order to retain any solid particle. The reaction products are continuously measured by Uras14/IR NO and CO/$CO_2$ analysers. In the soot oxidation experiments, only the CO/$CO_2$ gas analyser is used.

### 2.3. Soot characterization

As has been mentioned, all the soot samples formed have been characterized using different techniques: elemental analysis, determination of BET area, transmission electron microscopy (TEM), X-ray diffraction (XRD), Raman spectroscopy and X-ray photoelectron spectroscopy (XPS). The elemental analyses have been carried out in a Carlo Erba CHNS-O EA1108 analyser. A Quantachrome AUTOSORB-6 gas adsorption analyser is used for the surface area analyses with $N_2$ at 77 K. TEM images have been obtained using a JEOL JEM-2010 microscopy. XPS analyses are made in a VG-Microtech Mutilab 3000 analyser, XRD analyses in a Seifert JSO-DEBYEFLEX 2002 model and for Raman analyses, a Jobyn Yvon Horiba LabRam Spectrometer has been used.

## 3. Results and discussion

### 3.1. Soot formation

The results of gas composition, gas yield and soot yield obtained for different temperatures (1000–1200 °C) in the $C_2H_2$ pyrolysis experiments are shown in Figs. 3–5. The main gases analysed are $H_2$, $CH_4$, $C_2H_2$, $C_2H_4$, compounds with three ($C_3$) and four ($C_4$) carbon atoms and $C_6H_6$. As can be deduced from the results shown in Fig. 3, the conversion of acetylene increases with temperature, varying from 52% at 1000 °C up to 81% at 1200 °C. On the other hand, an increase in the temperature of soot formation leads to an increase in $H_2$ concentration, which

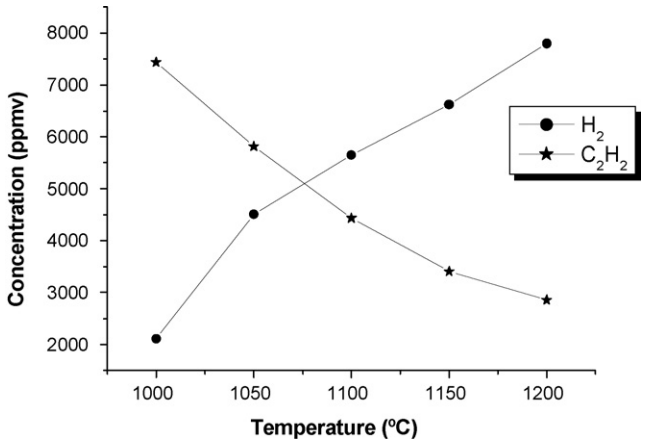


Fig. 3. Outlet gas composition ($H_2$ and $C_2H_2$) in the $C_2H_2$ pyrolysis experiments made for an inlet $C_2H_2$ concentration of 15,000 ppmv, in the 1000–1200 °C temperature range.

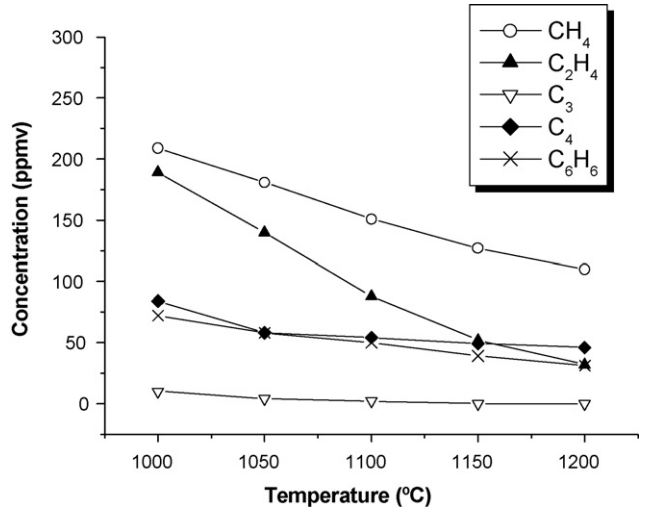


Fig. 4. Outlet gas composition ($CH_4$, $C_2H_2$, $C_3$, $C_4$ and $C_6H_6$) in the $C_2H_2$ pyrolysis experiments made for an inlet $C_2H_2$ concentration of 15,000 ppmv, in the 1000–1200 °C temperature range.

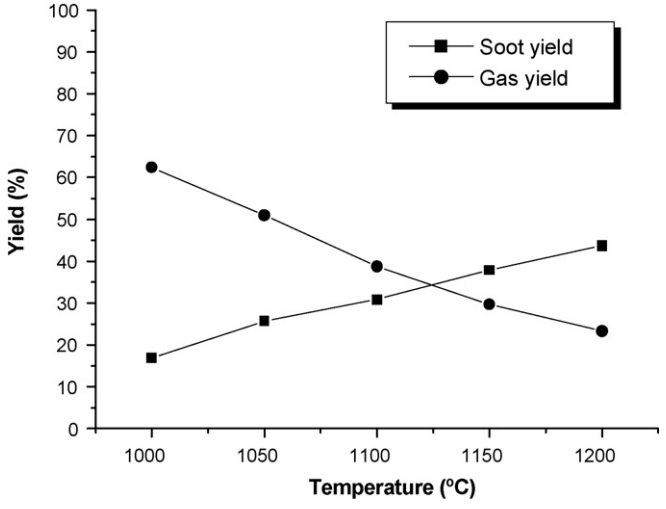


Fig. 5. Soot and gas yields obtained in the $C_2H_2$ pyrolysis experiments made for an inlet $C_2H_2$ concentration of 15,000 ppmv, in the 1000–1200 °C temperature range.

is the main gas product in all experiments. However, concentrations of the other gases analysed decrease with increasing temperature (Fig. 4). With respect to the gas and soot yields, they are defined as the percentage of the amount of carbon in the gases and soot, respectively, related to the amount of carbon that goes into the reactor. Fig. 5 shows that, increasing the temperature, the soot yield increases and, therefore, the gas yield decreases. The increase of soot yield with the temperature has been previously reported in the literature [18–21].

### 3.2. Soot reactivity

Experiments of the interaction soot–$O_2$ and soot–NO have been carried out in order to study the reactivity of the different soot samples formed and to further relate it with the characteristics of the corresponding soot.

#### 3.2.1. Soot–$O_2$ interaction

Several investigations have been carried out about the soot oxidation process in order to study the mechanisms of soot oxidation [22–24].

In this work, experiments of the interaction between the soot samples formed and oxygen have been carried out for an inlet oxygen concentration of 500 ppmv and for a temperature of 1000 °C. The outlet gases continuously analysed are CO and $CO_2$. During the experiments, carbon is mainly lost from the particles in the form of CO and $CO_2$. The carbon mass in the reactor at any time was calculated from the measured time variation of CO and $CO_2$ concentrations in ppm ($C_{CO}$ and $C_{CO_2}$, respectively) of the exhaust gas. In this way, the total initial amount of carbon (in mol) in the reactor, $N_{C_0}$, was defined as:

$$N_{C_0} = F_T \times 10^{-6} \int_0^{\infty} (C_{CO} + C_{CO_2})\, dt \quad (1)$$

where $F_T$ is the outlet flow expressed in mol per unit time and is expressed by the following equation:

$$F_T = \frac{Q\,P}{R_g\,T} \quad (2)$$

where $Q$ is the feeding flow rate, $P$ the reactor pressure, $R_g$ the universal gas constant in appropriate units and $T$ is the reactor temperature.

The amount of carbon (in mol) in the reactor at any time is calculated as:

$$N_C = N_{C_0} - F_T \times 10^{-6} \int_0^{t} (C_{CO} + C_{CO_2})\, dt \quad (3)$$

Therefore, the carbon mass in the reactor at any time, $W_C$, is determined as:

$$W_C = N_C\, M_C \quad (4)$$

where $M_C$ is the atomic mass of carbon.

In this way, the evolution of carbon conversion accumulated ($X_C$) as a function of time can be calculated for all experiments. These results for the soot samples obtained at different temperatures are shown in Fig. 6. As can be observed, higher $X_C$ values are reached with the soot samples formed at lower temperatures.

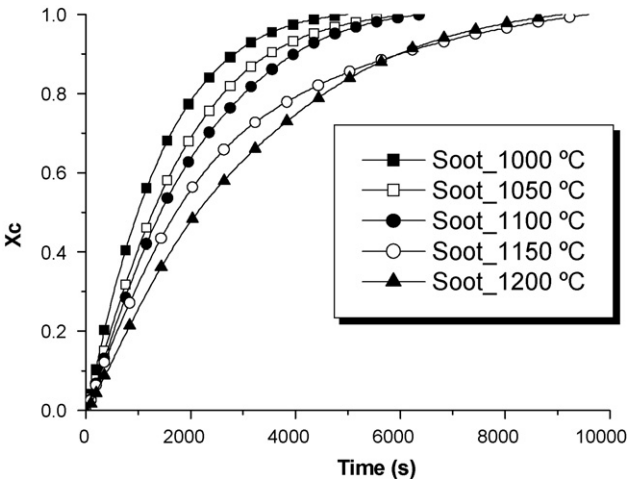


Fig. 6. Evolution of carbon conversion as a function of time in the soot oxidation experiments ([$O_2$] = 500 ppmv; $T$ = 1000 °C).

In order to compare the reactivities of the different soot samples, it has been considered interesting to use a simple particle kinetic model that fits with good accuracy the experimental data of the evolution of carbon conversion with time.

The particle model that there is used for describing this non-catalytic gas–solid reaction is the "shrinking core model" [25,26]. Its simplicity makes it adequate for the description of many heterogeneous, non-catalytic gas–solid reactions. Taking into account the experimental system, a constant gas concentration on the soot particle surface can be assumed. The experimental results fit with good accuracy to the following equation:

$$\frac{t}{\tau} = 1 - (1 - X_C)^{1/3} \quad (5)$$

that would correspond to the equation of the shrinking core model assuming a decreasing particle size and chemical reaction control. From this equation, using the carbon conversion values at any time, it is possible to calculate the so-called in the model, carbon complete conversion time, $\tau$.

The values of $\tau$ are calculated, according to Eq. (5), from the fitting of the experimental data of up to 95% carbon conversion. These $\tau$ values are inversely related to the solid reactivity. The $\tau$ values obtained for the soot samples formed at different temperatures are summarized in Table 1. It can be observed that the soot samples formed at lower temperatures have lower $\tau$ values, and thus, are more reactive towards $O_2$.

Table 1
Carbon complete conversion time in the soot oxidation experiments

| Soot samples | $\tau$ (s) |
|---|---|
| Soot_1000 °C | 5,406 |
| Soot_1050 °C | 6,636 |
| Soot_1100 °C | 7,469 |
| Soot_1150 °C | 9,573 |
| Soot_1200 °C | 11,211 |

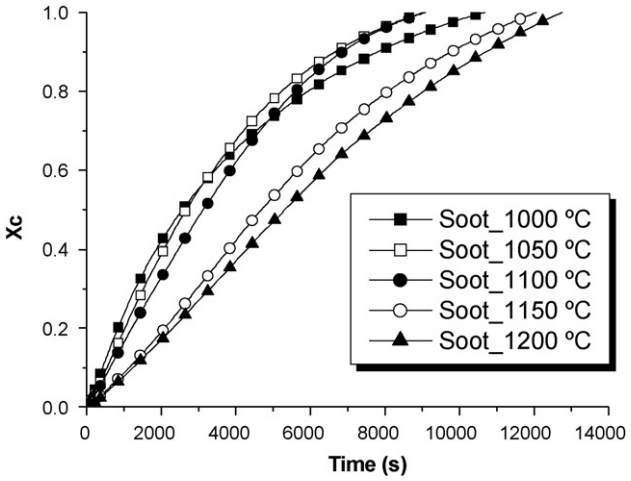


Fig. 7. Evolution of carbon conversion as a function of time in the interaction soot–NO experiments ([NO] = 2000 ppmv; $T$ = 1000 °C).

### 3.2.2. Soot–NO interaction

The great interest in reducing the emissions of nitrogen oxides has led to a large amount of work on the kinetics and mechanisms of reduction of NO by different carbonaceous solids [e.g. 3–5,27].

In this work, the interaction between the soot samples formed and NO has been studied for an inlet NO concentration of 2000 ppmv and a temperature of 1000 °C. The gases continuously analysed are CO, $CO_2$ and NO. From the concentration values obtained it is possible to calculate the carbon conversion and the NO conversion as function of time. These results are shown in Figs. 7 and 8, respectively. Although the NO conversions reached with all the soot samples are very low (less than 0.1), the soot samples formed at lower temperatures exhibit higher reactivities and lead to higher NO conversions. It should be noted in Fig. 8 that NO conversion decreases with run time because $W_C$ also decreases. In the same way as in soot oxidation experiments (using Eq. (5)), it is possible to calculate the carbon complete conversion time in the soot–NO interaction tests

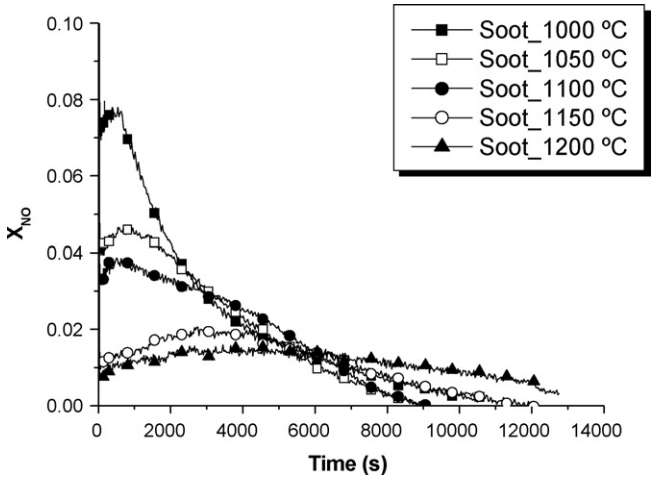


Fig. 8. Evolution of NO conversion as a function of time in the interaction soot–NO experiments ([NO] = 2000 ppmv; $T$ = 1000 °C).

Table 2
Carbon complete conversion time in the interaction soot–NO experiments

| Soot samples | $\tau$ (s) |
|---|---|
| Soot_1000 °C | 14,646 |
| Soot_1050 °C | 12,200 |
| Soot_1100 °C | 13,294 |
| Soot_1150 °C | 17,501 |
| Soot_1200 °C | 19,433 |

(Table 2). At any time, the amount of NO (in mol) reacted is similar to the moles of carbon converted. The soot samples formed at higher temperatures (1150 and 1200 °C) have higher $\tau$ values, and therefore they are the less reactive soot samples towards NO. On the other hand, as can be observed in Tables 1 and 2, the $\tau$ values are higher in the soot–NO interactions. Therefore, the soot samples are more reactive towards $O_2$ than towards NO.

## 3.3. Soot characterization

### 3.3.1. Elemental analysis

Table 3 shows the results of the elemental analyses of the different soot samples formed, as well as the C/H ratio in molar basis. The main element in the soot samples is carbon, more than 94% in all cases. The values of C/H ratio obtained are similar to the values observed by other authors [28]. It is worth noting that higher soot formation temperatures result in higher carbon contents and lower hydrogen contents. Thereby, the C/H ratios are higher at high temperatures. As has been reported in literature, the hydrogen content is directly related to the availability of active sites of the solid and so, to its reactivity [29–31]. This is in agreement with the results obtained (Figs. 6–8) because the soot samples formed at lower temperatures (1000 and 1050 °C), are the most reactive soot samples.

### 3.3.2. Surface area analysis

The surface area of a solid is also related to its reactivity. Several references state that soot particles are essentially nonporous, or have only limited porosity [32,33]. In the present study, the surface areas of the soot samples have been determined by nitrogen adsorption at 77 K and further calculated using the Brunauer–Emmett–Teller (BET) adsorption isotherm model. The results are summarized in Table 4. As can be observed, the area values of the soot samples are significantly low, being of the same order of magnitude as their external surfaces. The soot with the highest surface area is the one formed at 1050 °C, with 80.3 $m^2$/g. At higher temperatures, the surface area decreases considerably. As has been reported in literature [18,22,28], soot is a not microporous solid, and increasing temperature, a graphitization process occurs and can lead to lower surface area values.

### 3.3.3. Transmission electron microscopy (TEM)

TEM analyses have been carried out in order to deduce the microstructure of the different soot samples formed. The TEM images of these soot samples are shown in Fig. 9. It can be observed in the TEM micrographs obtained that soot has the appearance of chain-like aggregates composed of several tens or

Table 3
Elemental analysis and C/H ratio (molar basis) of the soot samples formed

| Soot samples | Elemental analysis (wt%) (dry basis) | | | | C/H (molar basis) |
|---|---|---|---|---|---|
| | C | H | N | S | |
| Soot_1000 °C | 94.90 | 0.30 | 0.00 | 0.00 | 26.36 |
| Soot_1050 °C | 95.51 | 0.36 | 0.00 | 0.00 | 22.11 |
| Soot_1100 °C | 97.53 | 0.17 | 0.00 | 0.00 | 47.81 |
| Soot_1150 °C | 98.65 | 0.14 | 0.00 | 0.00 | 58.72 |
| Soot_1200 °C | 97.95 | 0.16 | 0.00 | 0.00 | 51.02 |

hundred of sub-units, known as monomers or spherules. Low- and high-resolution transmission electron microscopy have been relied upon as the primary diagnostic for soot nanostructure [6,10,11,14–17,34–36]. Soot particles often occur as fractal aggregates with sizes up to several hundred nanometres, built up from primary particles with sizes of 5–50 nm, approximately [15–17,37].

Particle size is one important structural parameter of soot that is often assessed with microscopy or scattering techniques. The current methodology for soot primary particle size determination is through analysis of TEM micrographs. In this case, for each soot, an average size of the particles has been obtained from the TEM images. Two particle size ranges can be clearly distinguished: 150–220 nm for the soot samples formed at 1000 and 1050 °C, and 75–110 nm, for the soot samples formed from 1100 to 1200 °C. Therefore, the particle average size decreases when the soot formation temperature increases. These morphological phenomena are attributed to the shrinkage of the outer shell due to the growth and alignment the grapheme sheets [38–40]. This process converts the initially amorphous soot material to a progressively more graphitic carbon material with some decrease in particle size.

The soot particles appear to be encapsulated aggregates of highly defective carbon “onions”, presenting a graphitic structure (Fig. 9). These onion-like structures are made from parallel grapheme sheets arranged with their basal planes perpendicular to the radii of the structures. These have been also observed in the literature [12–14,41]. Several researchers [13,34] even distinguish clearly two parts: an inner core, composed of several fine particles of 3–4 nm in diameter, and an outer shell, composed of microcrystallites with periodic orientation of carbon sheets, or a so-called graphitic structure. In order to prove the existence of the graphitic outer shell, X-ray photoelectron spectroscopy (XPS) analyses of the soot samples formed have been made. XPS is widely used to study the electronic structure and can be applied to the structural characterization of carbon materials

Table 4
BET surface area ($m^2$/g) of the soot samples formed

| Soot samples | Surface area ($m^2$/g) |
|---|---|
| Soot_1000 °C | 52.8 |
| Soot_1050 °C | 80.3 |
| Soot_1100 °C | 70.4 |
| Soot_1150 °C | 58.1 |
| Soot_1200 °C | 39.8 |

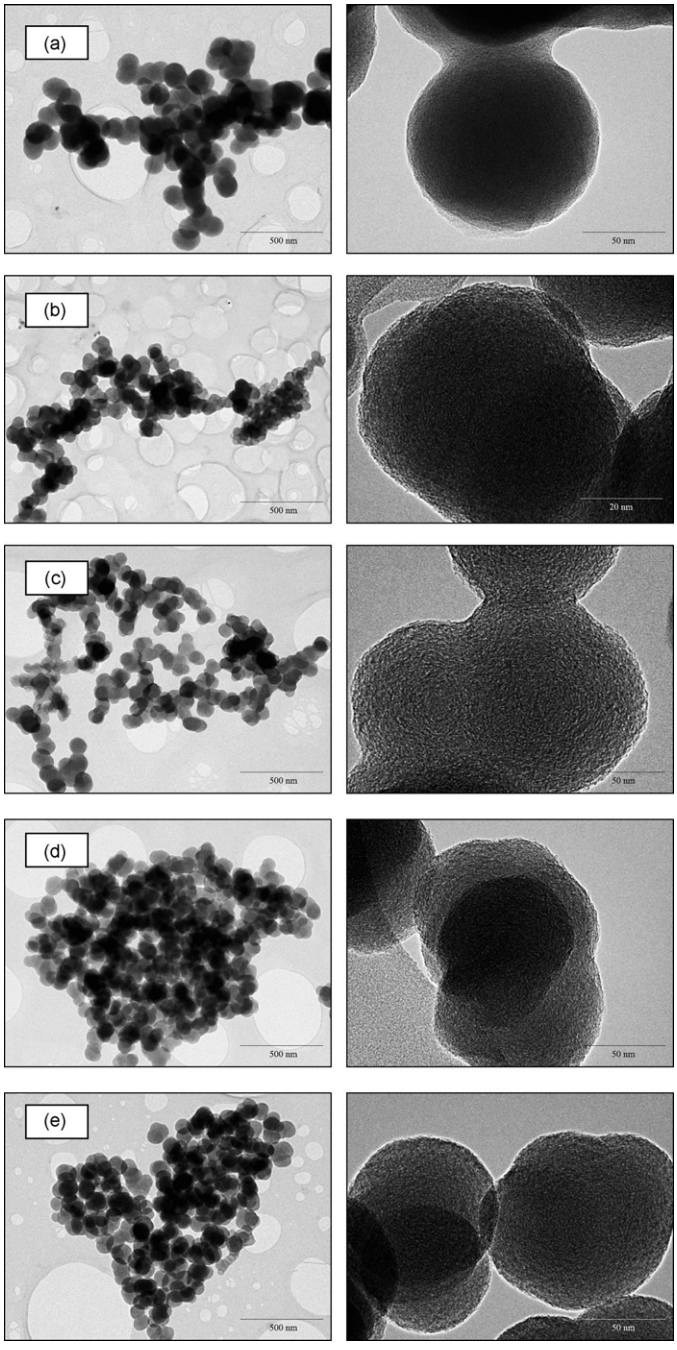


Fig. 9. TEM images of the soot samples obtained at different temperatures: (a) 1000 °C; (b) 1050 °C; (c) 1100 °C; (d) 1150 °C; (e) 1200 °C.

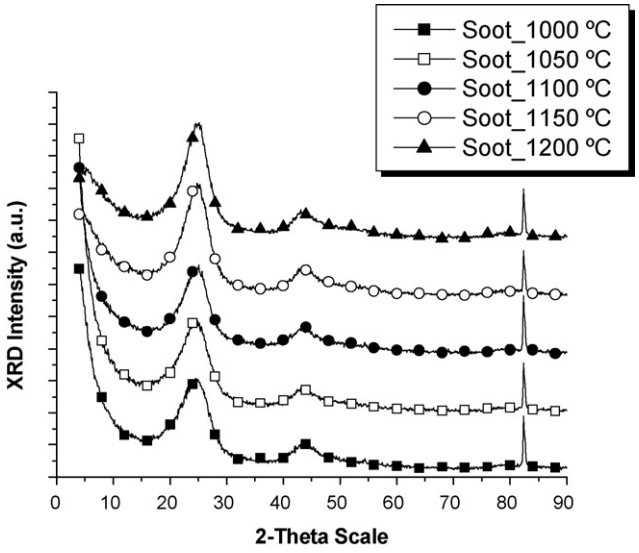


Fig. 10. Comparison of the X-ray diffractograms of the soot samples obtained at different temperatures.

[42,43]. This technique allows quantifying the carbon surface compounds existing in the soot samples. It can be noted from the results obtained that the main carbon surface compound in all the soot samples studied is graphite (more than 90% in all cases). These results agree with the presence of the graphitic outer shell previously mentioned. XPS analyses have also shown that most carbon atoms of the soot are in form of $sp^2$ hybridization, C–C chains or C–H [44].

### 3.3.4. X-ray diffraction (XRD)

X-ray diffraction is a non-destructive and well-established technique with good reproducibility. X-ray scattering techniques have been widely used for the study of size and structure of molecules and clusters [12,41,45–48]. Fig. 10 compares the diffractograms of the different soot samples generated. Diffractograms have been collected from 5° to 90°. All the soot samples present an overall similar shape of diffractogram. The most prominent peak is the (0 0 2) Bragg reflex, found at 25° on the $2\theta$-scale. The (0 0 2) peak position reflects the distance between the grapheme sheets. The (1 0 0) reflex is found at about 44°. Left aside the (0 0 2) reflex, the aliphatic γ-sideband is found at about 20°. This band is attributed to aliphatic side chains [48,49]. The soot samples share these characteristics with graphite, although the crystallites in soot are very small, as indicated by broad Bragg reflexes. The (0 0 2) reflex and its γ-band side chain have been fitted with two Gaussian functions in order to determine the aromaticity of the soot by their relative scattering contributions, as shown in the literature [48–50]. The aromaticity is used to describe the ratio of carbon atoms in aliphatic side chains versus aromatic rings. The aromaticity ($f$) can be defined as:

$$f = \frac{A_{(0\,0\,2)}}{A_{(0\,0\,2)} + A_{\gamma}} \quad (6)$$

where $A_{(0\,0\,2)}$ and $A_{\gamma}$ are the areas under either Gaussian curves. The results of aromaticity for the different soot samples are shown in Table 5. It can be observed that soot aromaticity increases with increasing the formation temperature of the soot. The aromaticity is directly related to the crystalline carbon content and to the C/H ratio of the carbonaceous material [50]. The soot samples with higher aromaticity values are the more ordered soot samples and have the higher C/H ratios. These are the soot samples formed at higher temperatures. Therefore, the more reactive soot samples, that are the soot samples formed at lower temperatures, are the most disordered soot samples [34].

Table 5
Aromaticity of the soot samples formed

| Soot samples | $A_{0\,0\,2}$ | $A_{\gamma\text{-band}}$ | Aromaticity ($f$) |
|---|---|---|---|
| Soot_1000 °C | 1556 | 624 | 0.71 |
| Soot_1050 °C | 1520 | 587 | 0.72 |
| Soot_1100 °C | 1452 | 528 | 0.73 |
| Soot_1150 °C | 1875 | 500 | 0.79 |
| Soot_1200 °C | 1892 | 500 | 0.79 |

### 3.3.5. Raman spectroscopy

Raman spectroscopy is an appropriate tool for the investigation of carbon compounds, since their Raman spectra have been found to respond to changes in the microscopic structure of the carbon materials [51–55]. An analysis of the spectra allows the inference of internal physical characteristics of the samples such as the degree of the structural disorder [52]. The Raman spectra of the soot samples formed are shown in Fig. 11. The main features of the spectra are seen to be a band peaking about 1350 $cm^{-1}$, the D peak, and another band centred about 1590 $cm^{-1}$, the G peak. The two bands are broad and their intensities are close. Graphite exhibits a single Raman peak at 1580 $cm^{-1}$ (G peak) [51,52]. As the graphite becomes disordered within the carbon layers, the G peak broadens. When the level of disorder further increases, a new peak called the D peak arises. In this case, in the soot samples, the D and G peaks are similar and broad. Therefore, the structure and Raman spectra of the soot samples can be interpreted in terms of highly disordered graphitic structures, as can be observed in the TEM micrographs (Fig. 9). To further investigate the two characteristic D and G

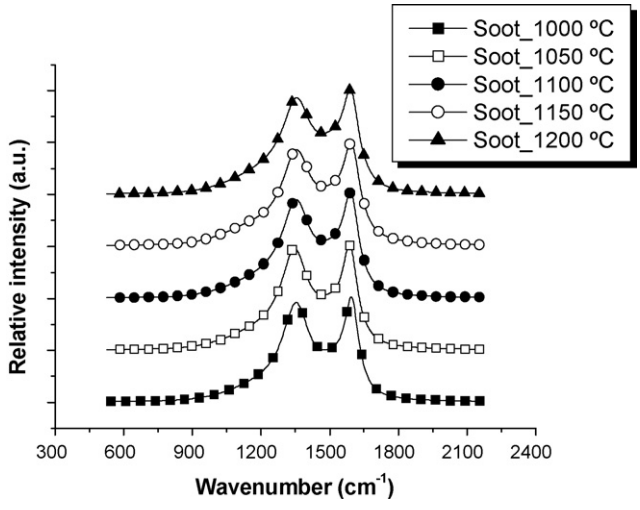


Fig. 11. Raman spectra of the soot samples formed.

Table 6
Results obtained from the Raman spectra of the soot samples formed

| Soot samples | D peak | | G peak | | $I_G/I_D$ |
|---|---|---|---|---|---|
| | Position ($cm^{-1}$) | FWHM ($cm^{-1}$) | Position ($cm^{-1}$) | FWHM ($cm^{-1}$) | |
| Soot_1000 °C | 1353.5 | 142.7 | 1596.1 | 74.2 | 1.047 |
| Soot_1050 °C | 1346.4 | 141.4 | 1588.8 | 79.8 | 1.024 |
| Soot_1100 °C | 1352.9 | 146.9 | 1593.3 | 81.6 | 1.057 |
| Soot_1150 °C | 1354.6 | 158.6 | 1596.4 | 89.7 | 1.058 |
| Soot_1200 °C | 1354.5 | 147.4 | 1593.2 | 82.8 | 1.086 |

peaks for the soot samples, the multiple Lorentzian method has been used to obtain the peak position of D and G bands, the full-width at half-maximum (FWHM), and the integrated intensity ratio ($I_G/I_D$). These results of fitting are summarized in Table 6. The positions of the D and G peaks are very close for all the soot samples. The value of the intensity ratio ($I_G/I_D$) is directly related to the graphitic order of the sample. The general trend is that the higher soot formation temperature, the higher graphitic order of the soot. This is in accordance with the results obtained from X-ray diffraction and elemental analysis.

## 4. Conclusions

The temperature in the formation of soot from acetylene pyrolysis has a clear influence on the yields to soot and the composition of the gases formed, as well as on the properties of the resultant soot samples. The reactivity behaviour of the soot samples is also related to their formation temperature, which is a key factor on their chemical composition, surface area and morphology, as can be observed in the characterization results obtained from elemental analysis, determination of BET surface area, TEM, XPS, XRD and Raman spectroscopy analyses.

The general trend is that the soot samples with higher reactivities towards $O_2$ and NO are the soot samples formed at lower temperatures. The results obtained in reactivity are in accordance with the characterization analyses. XRD and Raman spectroscopy show that the more ordered soot samples, and thus, the less reactive, are the soot samples formed at higher temperatures. Elemental analysis and surface area values of the soot samples also support these results.

## Acknowledgements

The authors express their gratitude to the MCYT (Project PPQ2003-02394) for financial support. Ms. M.P. Ruiz acknowledges the Spanish Ministry of Science and Education (MEC) for the award of a predoctoral grant (BES-2005-6898).

## References

[1] B.S. Haynes, H.G. Wagner, Soot formation, Prog. Energy Combust. Sci. 7 (1981) 229–273.
[2] I.M. Kennedy, Models of soot formation and oxidation, Prog. Energy Combust. Sci. 23 (1997) 95–132.
[3] I. Aarna, E.M. Suuberg, A review of the kinetics of the nitric oxide–carbon reaction, Fuel 76 (1997) 475–491.
[4] J.M. Commandré, B.R. Stanmore, S. Salvador, The high temperature reaction of carbon with nitric oxide, Combust. Flame 128 (2002) 211–216.
[5] M.J. Illán-Gómez, A. Linares-Solano, C.S.-M. de Lecea, J.M. Calo, NO reduction by activated carbons. 1: The role of carbon porosity and surface area, Energy Fuel 7 (1993) 146–154.
[6] R.L. Vander Wal, A.J. Tomasek, Soot nanostructure: dependence upon synthesis conditions, Combust. Flame 136 (2004) 129–140.
[7] L.E. Murr, K.F. Soto, A TEM study of soot, carbon nanotubes, and related fullerene nanopolyhedra in common fuel-gas combustion sources, Mater. Charact. 55 (2005) 50–65.
[8] W.J. Grieco, J.B. Howard, L.C. Rainey, J.B. Vander Sande, Fullerenic carbon in combustion-generated soot, Carbon 38 (2000) 597–614.
[9] W.J. Grieco, J.B. Howard, L.C. Rainey, J.B. Vander Sande, Spectroscopic and chemical characterisation of "fullerene black", Chem. Phys. Lett. 194 (1992) 62–66.
[10] C.R. Shaddix, A.B. Palotás, C.M. Megaridis, M.Y. Choi, N.Y.C. Yang, Soot graphitic order in laminar diffusion flames and a large-scale JP-8 pool fire, Int. J. Heat Mass Transf. 48 (2005) 3604–3614.
[11] Ch. Jäger, T. Henning, R. Schlögl, O. Spillecke, Spectral properties of carbon black, J. Non-Cryst. Solids 258 (1999) 161–179.
[12] A. Braun, F.E. Huggins, S. Seifert, J. Ilavsky, N. Shah, K.E. Kelly, et al., Size-range analysis of diesel soot with ultra-small angle X-ray scattering, Combust. Flame 137 (2004) 63–72.
[13] T. Ishiguro, Y. Takatori, K. Akihama, Microstructure of diesel soot particles probed by electron microscopy: first observation of inner core and outer shell, Combust. Flame 108 (1997) 231–234.
[14] S. Di Stasio, Electron microscopy evidence of aggregation under three different size scales for soot nanoparticles in flame, Carbon 39 (2001) 109–118.
[15] R.A. Dobbins, R.A. Fletcher, H.C. Chang, The evolution of soot precursor particles in a diffusion flame, Combust. Flame 115 (1998) 285–298.
[16] L.A. Sgro, G. Baseile, A.C. Barone, A. D'Anna, A. Minutolo, A. Borghese, et al., Detection of combustion formed nanoparticles, Chemosphere 51 (2003) 1079–1090.
[17] A.C. Barone, A. D'Alessio, A. D'Anna, Morphological characterization of the early process of soot formation by atomic force microscopy, Combust. Flame 132 (2003) 181–187.
[18] T. Mendiara, M.P. Domene, A. Millera, R. Bilbao, M.U. Alzueta, An experimental study of the soot formed in the pyrolysis of acetylene, J. Anal. Appl. Pyrol. 74 (2005) 486–493.
[19] A. Alexiou, A. Williams, Soot formation in shock-tube pyrolysis of toluene–*n*-heptane and toluene–*iso*-octane mixtures, Fuel 74 (1995) 153–158.
[20] A. Alexiou, A. Williams, Soot formation in shock-tube pyrolysis of toluene, toluene–methanol, toluene–ethanol, and toluene–oxygen mixtures, Combust. Flame 104 (1996) 51–65.
[21] T.H. Fletcher, J. Ma, J.R. Rigby, A.L. Brown, B.W. Webb, Soot in coal combustion systems, Prog. Energy Combust. Sci. 23 (1997) 283–301.
[22] B.R. Stanmore, J.F. Brilhac, P. Gilot, The oxidation of soot: a review of experiments, mechanisms and models, Carbon 39 (2001) 2247–2268.
[23] H. Jung, D.B. Kittelson, M.R. Zachariah, Kinetics and visualization of soot oxidation using transmission electron microscopy, Combust. Flame 136 (2004) 445–456.
[24] A. Messerer, R. Niessner, U. Pöschl, Comprehensive kinetic characterization of the oxidation and gasification of model and real diesel soot

by nitrogen oxides and oxygen under engine exhaust conditions: measurement, Langmuir–Hinshelwood, and Arrhenius parameters, Carbon 44 (2006) 307–324.
[25] O. Levenspiel, Chemical Reaction Engineering, 3rd ed., Wiley, New York, 1999, pp. 393–440.
[26] J. Szekely, J.W. Evans, H.Y. Sohn, Gas–Solid Reactions, Academic Press, New York, 1976, pp. 65–107.
[27] Y.H. Li, L.R. Radovic, G.Q. Lu, V. Rudolph, A new kinetic model for the NO–carbon reaction, Chem. Eng. Sci. 54 (1999) 4125–4136.
[28] M.B. Fernandes, J.O. Skjemstad, B.B. Johnson, J.D. Wells, P. Brooks, Characterization of carbonaceous combustion residues. I: Morphological, elemental and spectroscopic features, Chemosphere 51 (2003) 785–795.
[29] K.J. Rockne, G.L. Taghon, D.S. Kosson, Pore structure of soot deposits from several combustion sources, Chemosphere 41 (2000) 1125–1135.
[30] M. Guerrero, M.P. Ruiz, M.U. Alzueta, R. Bilbao, A. Millera, Pyrolysis of eucalyptus at different heating rates: studies of char characterization and oxidative reactivity, J. Anal. Appl. Pyrol. 74 (2005) 307–314.
[31] M.L. Chan, J.M. Jones, M. Pourkashanian, A. Williams, The oxidative reactivity of coal chars in relation to their structure, Fuel 78 (1999) 1539–1552.
[32] M.S. Akhter, A.R. Chughtai, D.M. Smith, The structure of hexane soot. I: Spectroscopic studies, Appl. Spectrosc. 39 (1985) 143–153.
[33] H. Burtscher, S. Kuenzel, C. Hueglin, Structure of particles in combustion engine exhaust, J. Aerosol Sci. 26 (1995) 129–130.
[34] J.O. Müller, D.S. Su, R.E. Jentoft, J. Kröhnert, F.C. Jentoft, R. Schlögl, Morphology-controlled reactivity of carbonaceous materials towards oxidation, Catal. Today 102/103 (2005) 259–265.
[35] A. Braun, F.E. Huggins, N. Shah, Y. Chen, S. Wirick, S.B. Mun, et al., Advantages of soft X-ray absorption over TEM–EELS for solid carbon studies—a comparative study on diesel soot with EELS and NEXAFS, Carbon 43 (2005) 117–124.
[36] U. Mathis, R. Kaegi, M. Mohr, R. Zenobi, TEM analysis of volatile nanoparticles from particle trap equipped diesel and direct-injection spark-ignition vehicles, Atmos. Environ. 38 (2004) 4347–4355.
[37] M. Wentzel, H. Gorzawski, K.H. Naumann, H. Saathoff, S. Weinbruch, Transmission electron microscopical and aerosol dynamical characterization of soot aerosols, Aerosol Sci. 34 (2003) 1347–1370.
[38] Y.A. Kim, T. Hayashi, K. Osawa, M.S. Dresselhaus, M. Endo, Annealing effect on disordered multi-wall carbon nanotubes, Chem. Phys. Lett. 380 (2003) 319–324.
[39] H. Richter, J.B. Howard, Formation of polycyclic aromatic hydrocarbons and their growth to soot—a review of chemical reaction pathways, Prog. Energy Combust. Sci. 26 (2000) 565–608.
[40] L. Ci, H. Zhu, B. Wei, C. Xu, J. Liang, D. Wu, Graphitization behaviour of carbon nanofibers prepared by the floating catalyst method, Mater. Lett. 43 (2000) 291–294.
[41] W. Zhu, D.E. Miser, W.G. Chan, M.R. Hajaligol, Characterization of combustion fullerene soot, $C_{60}$, and mixed fullerene, Carbon 42 (2004) 1463–1471.
[42] P. Chen, F. Huang, S. Yun, Characterization of the condensed carbon in detonation soot, Carbon 41 (2003) 2093–2099.
[43] U. Kirchner, R. Vogt, C. Natzeck, J. Goschnick, Single particle MS, SNMS, SIMS, XPS, and FTIR spectroscopic analysis of soot particles during the AIDA campaign, Aerosol Sci. 34 (2003) 1323–1346.
[44] K. Takahiro, A. Terai, S. Oizumi, K. Kawatsura, S. Yamamoto, H. Naramoto, Amorphization of carbon materials studied by X-ray photoelectron spectroscopy, Nucl. Instrum. Methods Phys. Res. B 242 (2006) 445–447.
[45] W. Ruland, B. Smarsly, X-ray scattering of non-graphitic carbon: an improved method of evaluation, J. Appl. Cryst. 35 (2002) 624–633.
[46] F. Ossler, J. Larsson, Exploring the formation of carbon-based molecules, clusters and particles in situ detection of scattered X-ray radiation, Chem. Phys. Lett. 387 (2004) 367–371.
[47] C. Gardner, G.N. Greaves, G.K. Hargrave, S. Jarvis, P. Wildman, F. Meneau, et al., In situ measurements of soot formation in simple flames using small angle X-ray scattering, Nucl. Instrum. Methods Phys. Res. B 238 (2005) 334–339.
[48] A. Braun, N. Shah, F.E. Huggins, K.E. Kelly, A. Sarofim, C. Jacobsen, et al., X-ray scattering and spectroscopy studies on diesel soot from oxygenated fuel under various engine load conditions, Carbon 43 (2005) 2588–2599.
[49] L. Lu, V. Sahajwalla, C. Kong, D. Harris, Quantitative X-ray diffraction analysis and its application to various coals, Carbon 39 (2001) 1821–1833.
[50] R.E. Franklin, The structure of graphitic carbons, Acta Cryst. 4 (1951) 253–261.
[51] A. Sadezky, H. Muckenhuber, H. Grothe, R. Niessner, U. Pöschl, Raman microspectroscopy of soot and related carbonaceous materials: spectral analysis and structural information, Carbon 43 (2005) 1731–1742.
[52] R. Escribano, J.J. Sloan, N. Siddique, N. Sze, T. Dudev, Raman spectroscopy of carbon-containing particles, Vib. Spectrosc. 26 (2001) 179–186.
[53] P. Chen, F. Huang, S. Yun, Optical characterization of nanocarbon phases in detonation soot and shocked graphite, Diam. Relat. Mater. 15 (2006) 1400–1404.
[54] P. Roubin, C. Martin, C. Arnas, Ph. Colomban, B. Pégourié, C. Brosset, Raman spectroscopy and X-ray diffraction studies of some deposited carbon layers in Tore Supra, J. Nucl. Mater. 337–339 (2005) 990–994.
[55] R. Guzmán de Villoria, A. Miravete, J. Cuartero, A. Chiminelly, N. Tolosana, Mechanical properties of SWNT/epoxy composites using two different curing cycles, Compos. Part B 37 (2006) 273–277.